This is a post-peer-review, pre-copyedit version of an article published in International Journal of Metalcasting. The final authenticated version is available online at: http://dx.doi.org/10.1007/s40962-016-0069-8.

Using optical measurement to determine the Young's Modulus of sand-core materials

B. Griebel, D. Brecheisen, R. Ramakrishnan, W. Volk, Institute of metal forming and casting, Technische Universität München, Garching, Germany

Abstract

An optical measurement setup is used to determine the elastic modulus of chemically bonded sand as it is used in foundry applications. The surface of sand specimen is recorded by a stereo camera system during a 4-point-bending test. The images are used to calculate the material's deformation. Three different methods to compute the Young's Modulus are compared. One depending on the displacement data captured by the testing machine and two methods depending on the data recorded by the optical system. All methods were used to characterize four different sand-core materials with organic and inorganic binders. The optical methods are promising to give more accurate results, as they measure directly on the specimen's surface.

Keywords: optical measurement, core-sand, Young's Modulus, elastic modulus

1. Introduction

Weight reduction of casting parts, high functional integration and higher grades of automation are the challenges of light metal foundries today. In gravity and low pressure die casting this causes a rising number of high complex cores that need to be joined, transported and inserted in the die by a highly automated process.[1] During the casting process, thermal expansion of the sand cores results in shape distortion which can affect the geometrical accuracy of the product.[2] To understand and optimize these processes more and more simulations are used. Those simulations are highly sensitive to material properties, therefore the exact determination of elastic moduli for sand-core materials becomes necessary. For example Ignaszak et al. (2011) simulated a hot distortion test and used reverse engineering technics to estimate the elastic modulus and the thermal expansion coefficient of quartz sand bonded by furan resin.[3] A value of 10 GPa was determined. One also tried to determine the elastic modulus of quartz sand bonded by polyurethane resin (cold-box) with a dynamic mechanical analysis.[4] This attempt was not successful, so the authors used the force-displacement graph measured in a three-point-bending test to determine the Young's Modulus of 4.3 GPa at room temperature. The force-displacement graph is non-linear, so the determined modulus represents a secant modulus.

This paper shows a novel method for measuring the elastic modulus of chemically bonded sand by optical measurement. It is compared to the conventional method of using the displacement values measured by the testing device. Those displacement values are always affected by local material failure in the contact area between testing device and sand-core specimen as it can be seen in Figure 1. So the optical measurement has the advantage of eliminating those errors by measuring directly on the specimen's surface.

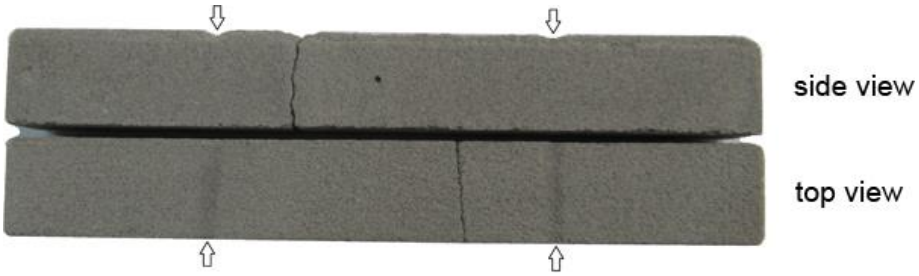

Figure 1: Inorganically 3-D-printed sand-core specimen after testing. The arrows highlight the local failure below the contact area with the 4-point-bending fixture.

2. Experimental setup

The test setup to determine the static elastic modulus of sand core materials is shown in Figure 2.

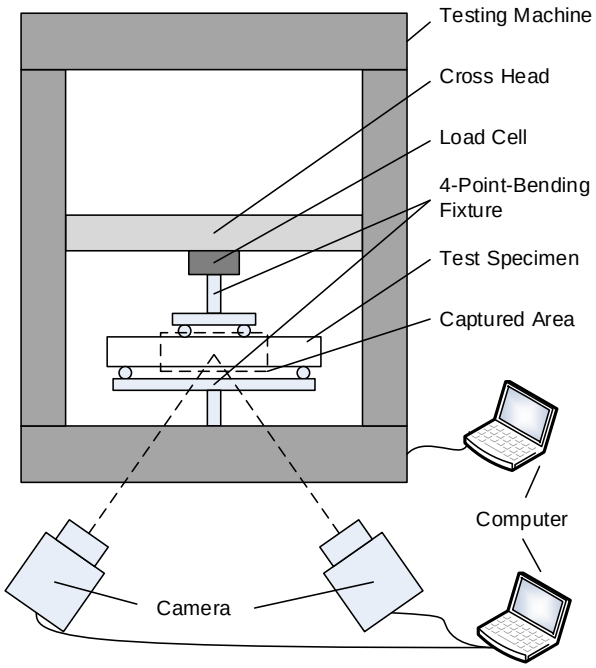

Figure 2: Test setup: A test specimen is bent in a testing machine with a 4-point-bending fixture. The surface of the specimen is recorded by two cameras of an optical measurement system.

A Zwick Z020 Universal Testing Machine (Zwick GmbH & Co. KG, Ulm) together with a 4-point-bending fixture is used to apply a flexural load on the test specimen. The 4-point-bending fixture is designed according to DIN EN 843 to ensure a constant and uniaxial torque between the upper supports.[5] The distance between the lower supports is 150 mm (5.9 in) and between the upper supports it is 75 mm (2.95 in). The applied force is measured by a force cell and the position of the cross head is detected by the testing machine. A computer is used to capture the cross head position and to control the movement of the machine so that the force is applied with a rate of 2 N/s.

An ARAMIS 5M Optical Measurement System (GOM mbH, Braunschweig) consisting of two 5 megapixel (2448x2050 pixels) digital cameras with a 50 mm (1.97 in) lens, a trigger unit and a computer is used to record the surface of the specimen. To record an area of 80x65 mm² (3.15 x 2.56 in²) the cameras are set up under an angle of 25° symmetrically to the surface normal. Dependent on the surface color and the light intensity, the exposure time is set to values between 15 and 100 ms. With 2 frames per second, the load force is increased by 1 N per shot.

Four different types of sand core materials were tested, to prove the method for varying surface structures and moduli. Table 1 shows an overview. Five specimens of each material were tested and used for evaluation.

Table 1: Sand core materials used in this study.

Name	Sand	Binder	Production Technologie
CI	Quartz sand, AFS 45	Inorganic (Sodium silicate)	Core-blowing
PI	Quartz sand, AFS 82	Inorganic (Sodium silicate)	3-D-Printing
CO	Quartz sand, AFS 47	Organic (Polyurethane)	Core-blowing
PO	Quartz sand, AFS 97	Organic (Furan)	3-D-Printing

CI was produced using a conventional core-blowing process on a small size core-blowing machine in the sand laboratory of BMW Group, Landshut. The sand was mixed with sodium silicate using a blade mixer. Afterwards the core was cured by drying in a hot core box and by hot air purge. PI was produced by a VX500 3-D-Printer (voxeljet AG, Friedberg) at the Institute of Metal Forming and Casting, Technische Universität München. In this process, an activator fluid is selectively printed in a sand bed containing quartz sand mixed with a dry sodium silicate binder. This way the core is generatively build up slice by slice. For curing, the core is dried in an oven for 1 h at 120 °C (392 °F). More detailed information on the printing process and the binder system was published in a recent paper.[6] CO was produced by Quarzwerke GmbH, Frechen using a small size laboratory core-blowing machine. The sand (H-S00011) was mixed with 0,7 % part 1 and 0,7 % part 2 of the two component resin. Afterwards the cores were cured by gassing with amine. PO material was also printed on a 3-D-Printer by voxeljet AG, Friedberg. In this process, the acid is mixed with the sand before it is recoated to the sand bed. Afterwards the furan resin is selectively printed to the current layer. The binder hardens within seconds after printing.

To measure the displacement while bending, the sand-core specimen is placed in the 4-point-bending fixture. Then the testing machine is started: After applying a preload of 20 N to ensure good contact between the fixture and the specimen, the force is increased by 2 N/s until the failure of the specimen. Once the preload is reached, the camera record is started manually. As the ARAMIS Software calculates all displacement values in reference to the first shot which is taken after applying the preload, all forces are also referenced to the preload. This is valid, as the bending line is a linear function with respect to the force according to the Euler-Bernoulli beam theory.

3. Calculation of displacements and strains inside the ARAMIS software

This section explains briefly how the calculation of displacements and strains is working with the equipment used for the examinations shown in this paper. Prior to the measurements the setup of the cameras is calibrated. Now the software knows the position of both cameras relative to each other and is able to determine the position of a feature, which is visible in both cameras. To recognize and to match those features in the images, the user has to define a grid of “facets”. A facet is a certain area of the images that contains a unique pattern (distribution of grey values) and therefore can be recognized in every image. It is represented by its center point. So a facet has to be big enough to contain a unique pattern of the recorded surface but as small as possible, to give a good resolution. To obtain good results with the sand-core surface, a facet of 20x20 pixel is chosen. They are overlapping by 10 pixels, so every 10 pixels a value is calculated. Figure 3 shows an example images overlain by the facet grid.

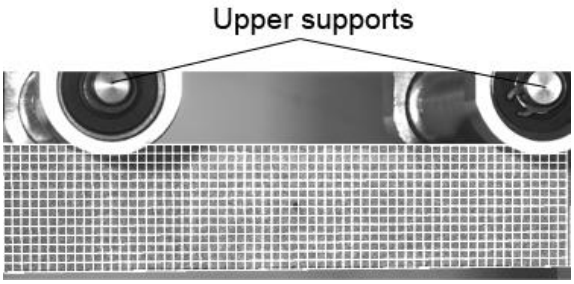

Figure 3: Example image of one of the cameras. In white the main field of facets.

Using the two images taken at the same time with the two cameras, the software can calculate the spatial position of the center point of each facet. To evaluate the displacement, the software simply compares the position of a facet at a certain time with its position in the first shot.

To calculate the local strains on a certain measuring point (facet center), the software uses the displacement values of a field of measuring points surrounding its center. As there are always more measuring points included in the evaluation than needed, the output value is determined by the least square method. When more displacement values are used to compute one strain value, less noise observed but also less resolution. To obtain reasonable values, a field of 15x15 facets (= 300x300 pixels) is chosen. Figure 4 shows an example displacement and strain output of the ARAMIS software.

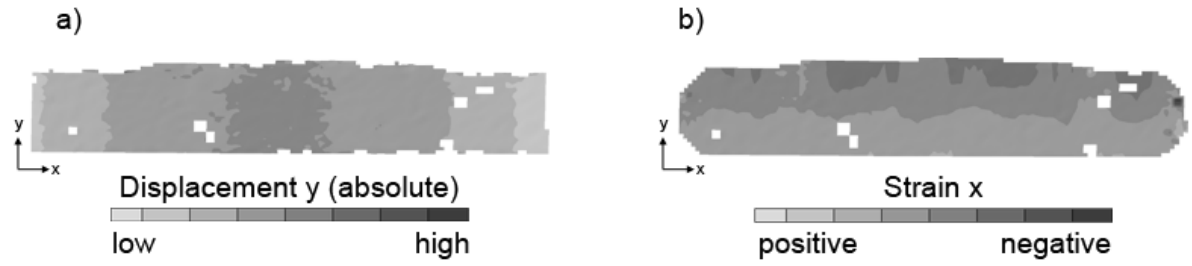

Figure 4: Examples of displacement and strain outputs. For directions x and y, see Figure 5.

4. Evaluation

As the tested materials do not show a distinct transition from elastic to plastic behavior, it is assumed, that the materials deform completely elastic until their sudden fracture. Therefore the elastic modulus is always calculated as the stress (σ) divided by the total strain (ϵ_{tot}) (Equation 1).

$$E = \frac{\sigma}{\epsilon_{tot}} \qquad \text{Equation 1}$$

The fracture stress (σ_{4PB}) is calculated according to Euler-Bernoulli beam theory from the maximum force F at fracture and the geometry introduced in Figure 5 (Equation 2). [7]

$$\sigma_{4PB} = \frac{3Fl_1}{bh^2} \qquad \text{Equation 2}$$

To calculate the Young's Modulus from the recorded data, three different methods were used and compared:

Cross Head Displacement

This method uses the cross head displacement data recorded by the testing machine to calculate a Young's Modulus. Assuming that core sand material can be treated as a homogeneous, ideal elastic material with small displacements, the elastic modulus can be calculated according to the Euler-Bernoulli beam theory (Equation 3).[7]

$$E_{CHD} = \frac{14\Delta F l_1^3}{bh^3 \Delta d_{CH}} \qquad \text{Equation 3}$$

Here E_{CHD} is the elastic modulus calculated by the cross head displacement. l_1 is the distance between a lower and an upper support on the same side and l_2 is the distance between the upper supports. b and h represent the width and the height of the specimens cross section. ΔF is the difference in load force and Δd_{CH} the difference in the displacement of the cross head.

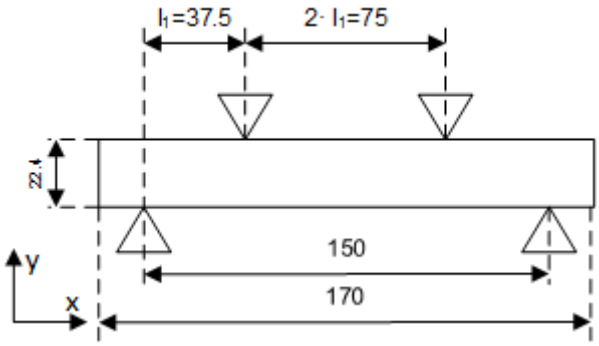

Figure 5: Schematic of the beam with coordinate system, distances between the supports and the measurement of the specimen. All measurements given in mm.

Due to settling and local failure of the sand material, the graph of load force versus cross head displacement is not a smooth line for low loading forces. Therefore ΔF cannot be referenced to zero load. Instead a line is fitted by least-square-method to the smooth part of the graph between 40% and 90% of the maximum force. In Figure 6 a force-displacement graph is plotted and the fitted line between 40% and 90% of the maximum force is highlighted.

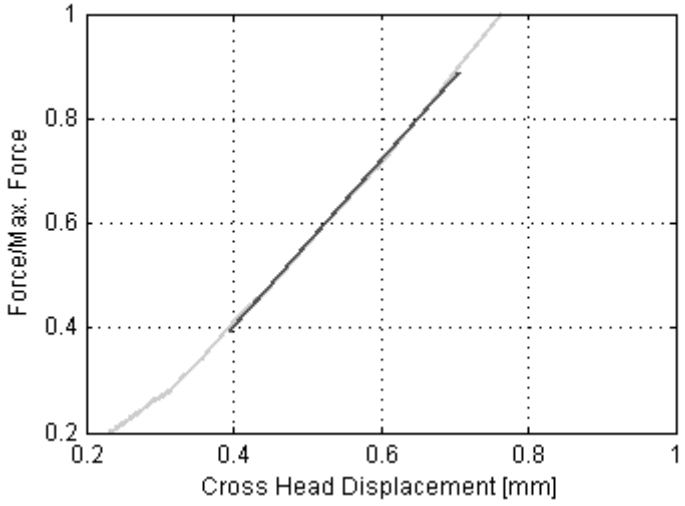

Figure 6: Relative Force vs. Displacement graph of a PI-specimen plotted in light grey. The fitted line between 40% and 90% of the maximum load force is plotted in dark grey.

Bending Line Curvature

Also according to the Euler-Bernoulli beam theory, the elastic modulus can be calculated as shown in Equation 4.[7]

$$E_{CU} = \frac{12 \cdot F l_1}{b h^3 \cdot \kappa} \qquad \text{Equation 4}$$

With κ representing the bending curvature of the sand specimen.

To obtain the curvature of a sand-core specimen, the average of all displacement values with the same x-component is calculated, so the displacement data is reduced to a one dimensional line. The torque between the upper supports is constant, which results in a constant curvature. Therefore a polynomial of second order is fitted to the measured bending line between the upper supports using the least square method. The second derivative of this polynomial is used as the curvature value to calculate E_{CU}. Figure 7 shows an example of the measured displacement values between the upper supports of one specimen and the fitted polynomial. This way a Young's Modulus can be determined for every shot, which corresponds to a certain load step. A single value for each specimen is calculated by building the average between 40% and 90% of the maximum load force.

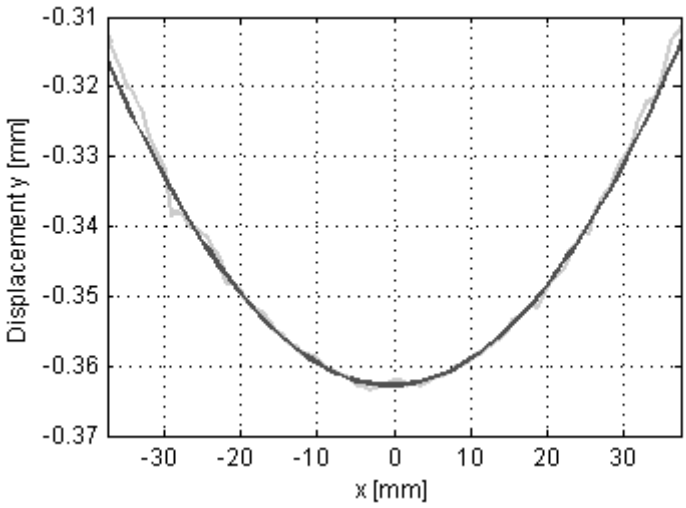

Figure 7: Optically measured y-displacement vs. x-coordinate of a PI-specimen in light grey. The fitted polynomial is plotted in dark grey.

Strain Calculation

The size of the field that is used to determine the local strains (see section 3) is almost half the size of the specimen's height. Nevertheless the obtained values are correct because the trend is expected to be linear over the beams height. And calculating a moving average over a linear function reproduces this function independent of the number of points that are used. This is only possible if the whole averaging window is covered by the specimen's surface, which is roughly the case for $6\,mm \leq y \leq 16\,mm$. Again for every point along the y-axis a value is calculated by building the average of all values between the upper supports with the same y-component. This produces a graph like the one that is plotted in Figure 8. To determine an elastic module, first a line is fitted to the values between $7\,mm \leq y \leq 15\,mm$, then the first derivative of this line is used to calculate the elastic module according to equation 5.[7]

$$E_{ST} = -\frac{12 \cdot Fl_1}{bh^3 \cdot m}$$ Equation 5

With m representing the slope of the strain.

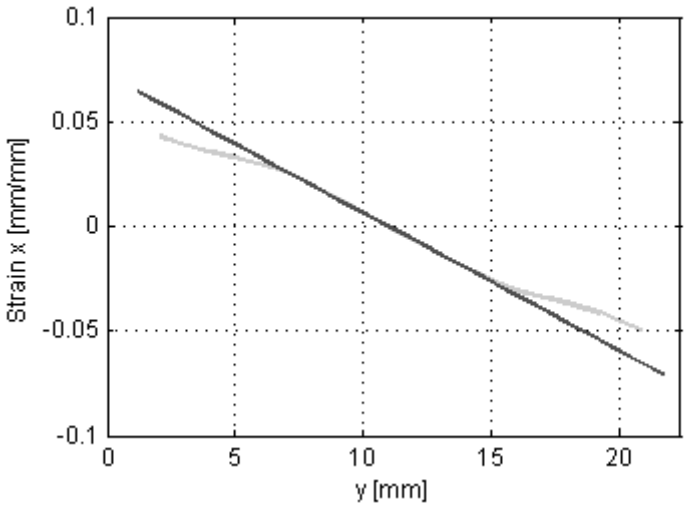

Figure 8: Optically measured x-strain plotted against y-coordinate of a PI specimen in light grey. The fitted line (7<y<15) is plotted in dark grey.

5. Results

Fracture Stress

The maximum force at the fracture of the specimens is recorded. Equation 2 is used to determine the fracture stress (σ_{4PB}). Figure 9 shows σ_{4PB} of the different sand-core materials. The error bar represents two standard deviations. PI is the material with the highest strength of 4.07 MPa. CI and CO have comparable strength values of 2.38 MPa and 2.90 MPa. Finally PO has the lowest strength of 1.36 MPa.

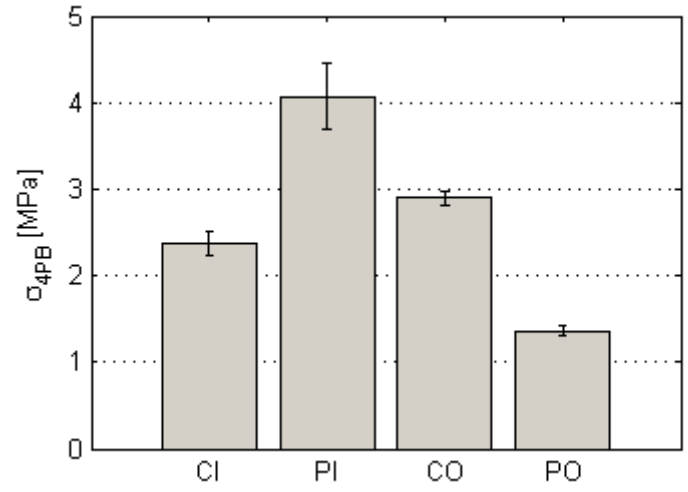

Figure 9: Fracture stress of sand-core materials measured by 4-point-bending test. The error bar represents twice the standard deviation.

Young's Modulus

Figure 10 shows the mean Young's Modulus E evaluated with the three methods mentioned for the four different materials. Also the noise is plotted by error bars, which have the size of two standard deviations. The values calculated by the method *Cross Head Displacement* are significantly lower than the values determined by optical measurements. For all materials, the difference between the two optical methods *Bending Line Curvature* and *Strain Calculation* is smaller than the standard deviation. The noise of the method *Strain Calculation* for the material CO is a lot bigger in comparison to the other materials. This is caused by a contrast of the surface structure, which is poor for CO. That leads to a poor recognition of the facets in the ARAMIS software and therefore to less valid calculation points, which greatly affects the quality of the strain result.

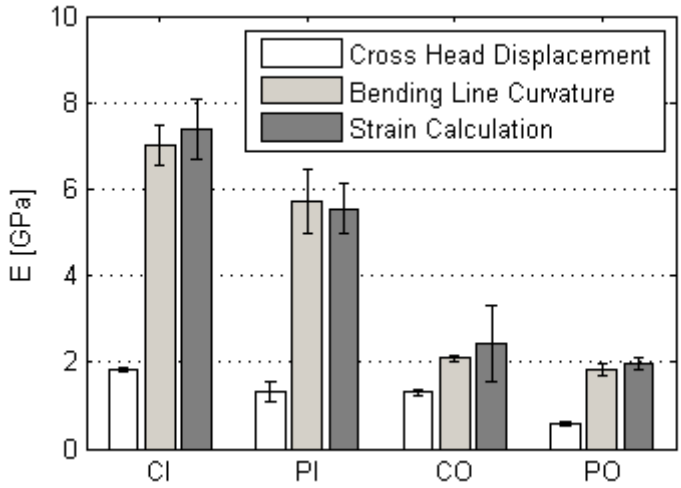

Figure 10: Mean Young's Modulus E evaluated with three different methods for all sand-core materials. The error bar represents two standard deviations.

Figure 11 and Figure 12 show the development of the Young's Modulus of one PI and one PO specimen during a bending test. The stiffness is plotted against the relative load force. The PI material shows a wave-like shape that is falling in total while the load is increasing. The wave-like shape was observed for all inorganic binders (PI and CI). The PO material also shows a decrease of apparent stiffness while the load is increasing, but it does not show any wave-like shape. This was observed for all organic (PO and CO) specimen.

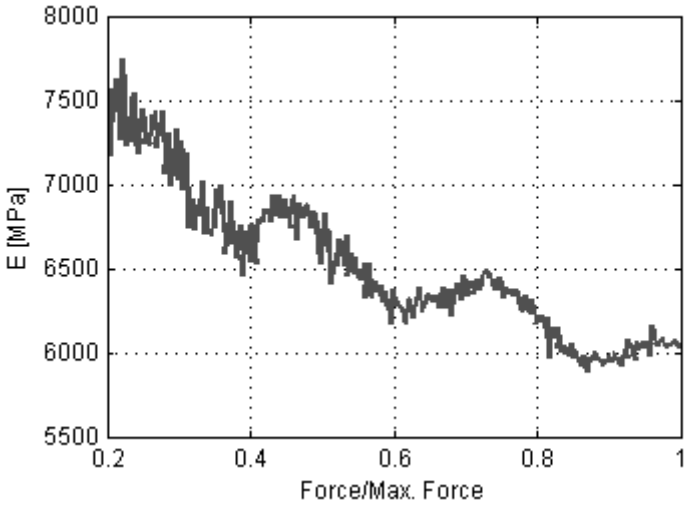

Figure 11: Young's Modulus E plotted against the relative force (Force/Max. Force) for one PI specimen.

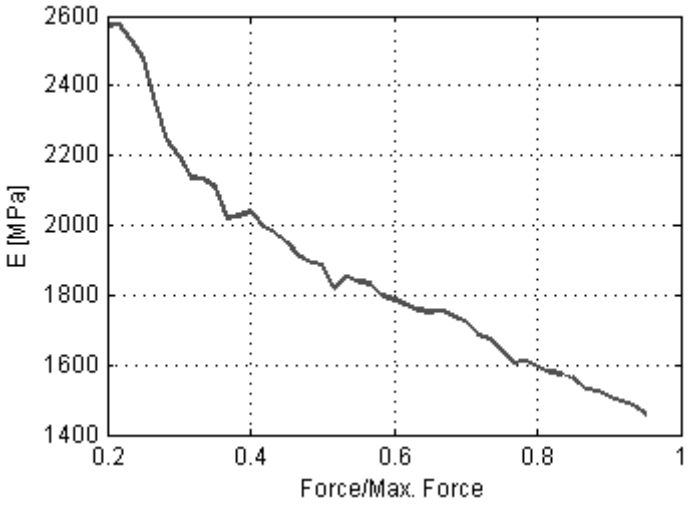

Figure 12: Young's Modulus E plotted against the relative force (Force/Max. Force) for one PO specimen.

6. Discussion

The fact that the values calculated by *Cross Head Displacement* are lower than the optically measured ones can be explained by the stiffness of the 4-Point-Bending-Fixture and also the effect of local material failure in the contact area between fixture and specimen. These effects are leading to overestimated displacement values, which are causing underestimated stiffness values. The optical system measures directly on the specimen's surface and is therefore not affected by those issues. Hence the values determined by optical measurement are assumed to be the "real" values. As a matter of fact, the strain values occurring are just big enough to be measured by this system. Therefore variation between individual values on the specimen's surface is rather big, which is the reason why good results are only obtained by building the average over the complete area between the upper supports. This is valid, because the torque in this area is constant. In case of the material CO there were not enough values due to the poor recognition of the surface structure, which results in a high standard variation of the strain values.

A comparison of the breaking stress and the average Young's Modulus of the different materials shows that the stiffness seems to be related mostly to the binder. PI and CI, which have comparable binders also have a comparable Young's Modulus. This is also true for PO and CO. On the other hand, the properties of the sand and the manufacturing methods seem to have an impact only on the strength of the materials.

Moreover the standard deviations of the Young's Modulus are only slightly bigger than the standard deviations of the breaking stress, which means that the optical measurement contributes only a small amount to the total noise. Most of it appears to arise from the material itself, as the force measurement is assumed to have a negligible noise.

All materials show a decreasing stiffness during the bending test, which could be interpreted as plasticity. In the case of PI and CI materials no plasticity is expected as they consist of quartz and sodium silicate, which are both materials that do not show any plasticity. Therefore the falling stiffness is assumed to be an effect of local failure. The wave-like shape in the stiffness vs. load graph of materials CI and PI cannot be explained yet.

In section 1 two values that were reported in literature are mentioned: 4 GPa for a cold-box system and 10 GPa for a furan system. Both of them are roughly in the same range as the results described in this paper. A more detailed comparison is difficult, as the Young's Modulus

depends mainly on the binder, its processing and storage. The cited literature gives only little information on those details.[3,4]

7. Conclusion and outlook

A method for determining the Young's Modulus of sand-core materials using an optical measuring system is described. As this system is measuring directly on the surface of the material, it is immune to errors caused by the unknown contact between the fixture and the specimens and the errors caused by the finite stiffness of the bending fixture itself. The method was successfully used to calculate the Young's Moduli of four different sand-core materials. All materials show a "plastic-like" behavior even though inorganically bound cores should not show any plasticity, as their components quartz and waterglass are known to have a brittle failure. It is assumed that this is caused by local failure.

Future work could address this issue by measuring for example the elastic behavior at cyclic loading. Furthermore elastic stiffness at higher temperatures could be measured with this method and a furnace with optical access. That data is essential to simulate the behavior of sand-core material during casting.

8. Acknowledgement

The authors would like to thank BMW Group, voxeljet AG and Quarzwerke GmbH for supporting the work by supplying sand-core materials.

9. References

1. Becker, H.-H., Rösch, R., Hansen, F., Jäger, G., Uhde, S., "Vollständig verkettete anorganische Kernfertigung in der Zylinderkopffertigung bei Volkswagen," *GIESSEREI*, vol. 101, no. 07, pp 30–36 (2014).
2. Bakhtiyarov, S.I., Sherwin, C.H., Overfelt, R.A., "Untersuchung des Heißverzugs von Phenolurethan Cold-Box Kernen," *GIESSEREI -PRAXIS*, 1-2/2007, pp 12–21 (2007).
3. Ignaszak, Z., Popielarski, P., Strek, T., "Estimation of Coupled Thermo-Physical and Thermo-Mechanical Properties of Porous Thermolabile Ceramic Material using Hot Distortion Plus Test," 2011, www.scientific.net.
4. N. N., "Abschlussbericht AiF-Vorhaben 14357/N1: Thermomechanisches Verhalten von Gießereisandkernen," (2007).
5. DIN, EN, "Hochleistungskeramik - Mechanische Eigenschaften monolithischer Keramik bei Raumtemperatur," 81.060.30, 843-5, Beuth Verlag GmbH, Berlin (2007), www.beuth.de; www.din.de.
6. Ramakrishnan, R. Dipl.-Ing, Volk, W. Prof. Dr.-Ing., Griebel, B. Dipl.-Ing., Günther, D. Dr.-Ing., "3D Printing of Inorganic Sand Moulds for Casting Applications," *Advanced Materials Research*, no. 1018, pp 441–449 (2014).
7. Gross, D., Hauger, W., Schnell, W., Schröder, J., Wall, W.A., "Technische Mechanik: Band 1: Statik," 9th ed., Springer-Verlag Berlin Heidelberg, Berlin, Heidelberg (2006).